Nitrate and Nitrite Ultraviolet Actinometers

Joseph J. Jankowski[1], **David J. Kieber**[*1] **and Kenneth Mopper**[2]

[1]State University of New York, College of Environmental Science and Forestry, Department of Chemistry, Syracuse, NY, USA and
[2]Washington State University, Department of Chemistry, Pullman, WA, USA

ABSTRACT

We developed nitrate and nitrite actinometers to determine radiant fluxes from 290 to 410 nm. These actinometers are based on the reaction of the photochemically generated OH radical with benzoic acid to form salicylic acid (SA) and *p*-hydroxybenzoic acid (pHBA). Actinometer development included determination of the temperature and wavelength dependence of the quantum yield for formation of SA and pHBA from nitrate and nitrite photolysis in air-saturated solutions. Quantum yields (at 25°C) for SA production from nitrate photolysis ranged from 0.00146 to 0.00418 between 290 and 350 nm, and from 0.00185 to 0.00633 for nitrite photolysis between 290 and 405 nm. The quantum yields for SA production were approximately 50–60% greater than quantum yields for pHBA production from nitrate and nitrite photolysis. For both actinometers, SA and pHBA formation was temperature dependent, increasing by approximately a factor of 2.2 from 0 to 35°C. Activation energies for SA formation varied with wavelength, ranging from 14.7 to 16.5 kJ mol^{-1} between 290 and 330 nm for the nitrate actinometer and 12.3 to 17.8 kJ mol^{-1} between 310 and 390 nm for the nitrite actinometer. Activation energies for pHBA formation were 2–11% higher. Wavelength-dependent changes in the quantum yield and activation energy for SA and pHBA formation from nitrate photolysis suggest multiple electronic transitions for nitrate from 290 to 350 nm. Quantum yields for OH radical formation from nitrate and nitrite photolyses were estimated from SA and pHBA quantum yields at 25°C. Wavelength-dependent OH quantum yields ranged from 0.007 to 0.014 for nitrate photolysis between 290 and 330 nm and from 0.024 to 0.078 for nitrite photolysis between 298 and 390 nm. The nitrate and nitrite actinometers can maintain initial rate conditions for hours, are insensitive to laboratory lighting, easy to use and extremely sensitive; the minimum radiant energy that can be detected in our irradiation system is approximately 10^{-9} einsteins.

INTRODUCTION

The determination of photochemical quantum yields is dependent on the accurate measurement of monochromatic radiant fluxes. Chemical actinometry is the most common method for determining radiant fluxes during photochemical studies, having an advantage over most instrumental methods because actinometers are able to measure the photon flux within the irradiated cell. The utility of an actinometer is based on its accuracy, sensitivity, linear dynamic range, reciprocity and ease of use. Additionally, for the study of photoprocesses occurring in water, the actinometer should be aqueous-based to minimize refractive index differences. Currently, potassium ferrioxalate actinometry (1) is the most common method used to determine monochromatic radiant fluxes. The potassium ferrioxalate actinometer (PFA)† is used to determine radiant fluxes from the UV out to visible wavelengths. Unfortunately, because PFA absorbs visible light, its analysis, which involves the complexation of ferrous iron and its subsequent absorbance detection, must be performed in a darkroom. The development of actinometers based on the photolysis of valerophenone (2) and *p*-nitroanisole (PNA) (3) has allowed for accurate measurement of UV radiant fluxes without the need for a darkroom. However, the sensitivity of these actinometers is limited because they are based on the loss, rather than the production, of a chromophore. To overcome the limitations of these actinometers, we developed nitrate and nitrite actinometers for radiant flux determinations from 290 to 405 nm. These actinometers are insensitive to laboratory lighting and quantify radiant fluxes based on the production of highly fluorescent and absorptive analytes.

The aqueous photochemistry of nitrate has been the focus of numerous studies, with emphasis on elucidation of nitrate's electronic transitions (4–8) and the mechanism and products of nitrate photolysis (9–15). Nitrate has two principal absorption bands, the first is an intense $\pi \rightarrow \pi^*$ band (4) occurring in the far UV ($\epsilon_{max} = 9500\ M^{-1}\ cm^{-1}$ at 201 nm), while the second is a weak absorption band centered at 302 nm ($\epsilon_{max} = 7.14\ M^{-1}\ cm^{-1}$). The photolysis of nitrate in the UVB (290–320 nm) has also been examined for its

---

*To whom correspondence should be addressed at: State University of New York, College of Environmental Science and Forestry, Department of Chemistry, 1 Forestry Drive, Syracuse, NY 13210, USA. Fax: 315-470-6856; e-mail: djkieber@mailbox.syr.edu

role in the marine nitrogen cycle (11) and as a source of the hydroxyl radical (12–14,16). The direct photolysis of nitrate proceeds *via* two pathways (10):

$$NO_3^- + h\upsilon \rightarrow NO_2 + O^- \qquad (1)$$

$$NO_3^- + h\upsilon \rightarrow NO_2^- + O(^3P) \qquad (2)$$
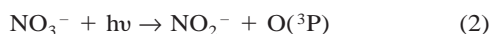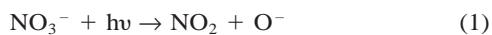
Approximately 90% of nitrate photolysis proceeds through pathway 1 (14), with the O^- radical undergoing rapid protonation to form the hydroxyl radical (OH). Approximately 10% of nitrate photolysis occurs through the second pathway (14), where the $O(^3P)$ atom is thought to react with molecular oxygen to form ozone.

Nitrite has also been studied to determine its electronic transitions (17) and mechanism of photochemical decay (13,18,19). Nitrite has three absorption bands in the UV (17). The first involves a strong $\pi \rightarrow \pi^*$ absorption with a maximum at 220 nm, and the other two correspond to $n \rightarrow \pi^*$ transitions that occur in the UVB and UVA (320–400 nm), with one defined absorption maximum at 354 nm (ϵ_{max} = 22.7 M^{-1} cm^{-1}). Nitrite undergoes direct photolysis, leading to production of the hydroxyl radical (18):

$$NO_2^- + h\upsilon \rightarrow NO + O^- \qquad (3)$$

$$O^- + H_2O \rightarrow OH + OH^- \qquad (4)$$
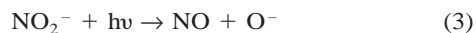
Quantum yields for hydroxyl radical production from nitrate and nitrite photolysis are low ($\sim$0.01) (12–14,19). As a consequence, nitrate and nitrite photolyses can be used for long-term irradiations (*ca* hours) without altering the solution composition. This is in contrast to loss-based actinometers that require sensitizers or quenchers to manipulate reaction rates (2,3). The nitrate and nitrite photolyses are extremely sensitive because the OH radical is trapped to form highly chromophoric and fluorescent products. This allows for the quantification of low radiant fluxes during short-term irradiations (*ca* minutes).

We developed the nitrate and nitrite actinometers using benzoic acid (BA) as the scavenger of the OH radical, leading to the formation of monohydroxybenzoic acids (20,21). The mechanism and products of these reactions are well documented (22–26). A chromatographic method (27) was used to quantify *ortho-* (salicylic acid, SA) and *para*-hydroxybenzoic acid (pHBA). Using this technique, wavelength-dependent quantum yields were determined for the formation of SA and pHBA from the photolysis of the nitrate or nitrite actinometer solutions. This method was also used to determine the temperature dependence of SA or pHBA formation at several wavelengths. Additionally, a batch fluorescence technique was developed at the later stages of this study to provide an alternative method for quantifying SA production in the actinometer solutions.

MATERIALS AND METHODS

Chemicals. Sodium nitrate ($\geq$99.995%), pHBA and *m*-hydroxybenzoic acid (mHBA) ($\geq$99%), valerophenone (>99%) and potassium oxalate monohydrate ($\geq$99%) were obtained from Aldrich Chemical Company (Milwaukee, WI). Sodium nitrite (>99%) was purchased from Fluka Chemical (Buchs, Switzerland). The ACS reagent-grade phenanthroline was obtained from Fisher Scientific (Pittsburgh, PA). Salicylic acid ($\geq$99.5%) and reagent-grade sodium bicarbonate, sodium acetate, BA, monobasic potassium phosphate and phosphoric acid were purchased from J. T. Baker, Inc. (Phillipsburg, NJ). Ferric

chloride was purchased from Mallinckrodt Chemical, Inc. (Paris, KY). Distilled-in-glass, high purity methanol and acetonitrile were obtained from Baxter Diagnostics, Inc. (McGaw Park, IL). All chemicals were used as received, with the exception of BA that was recrystallized three times from high purity laboratory water.

All solutions were prepared with water from a Millipore water purification system (Millipore Corp., Chicago, IL) having a resistance >18 MΩ cm. The water purification system consisted of filtration/dechlorination cartridges followed by a Milli-RO (reverse osmosis) system, a four cartridge Milli Q system (Super C carbon cartridge, two ion-exchange cartridges, and an Organex Q cartridge) and final filtration through a 0.2 μm Whatman Polycap AS capsule (Fisher Scientific). All solutions in this study were prepared with Milli Q water in borosilicate glassware and stored in the dark at 4°C.

Quantum yield determinations were made in an air-saturated 2.5 mM sodium bicarbonate solution containing 1 mM BA and either 10 mM sodium nitrate or 1 mM sodium nitrite. The pH of these solutions was 7.2. These solutions were stable for at least 45 days when stored in the dark and refrigerated.

The potassium ferrioxalate used for chemical actinometry was prepared by adding three parts potassium oxalate (1.5 M) to one part ferric chloride (1.0 M). The resulting precipitate was recrystallized three times with Milli Q water and dried in a desiccator. An 8.7 mM aqueous potassium ferrioxalate solution in 0.05 M sulfuric acid was prepared from these crystals as needed.

HPLC. The HPLC system consisted of an Eldex model B-100-S single piston pump (Eldex Laboratories, Menlo Park, CA) connected to an Anspec Bio-Merge gradient mixer (The Anspec Co., Ann Arbor, MI), a 0–5000 psi pressure gauge (C and H Sales, Vineland, NJ), a two-position, six-port injection valve (Valco Instruments Co., Houston, TX) with a 100 μL loop and a Waters RCM radial compression cartridge holder with a Waters 8 $\times$ 100 mm Radial Pak cartridge containing 4 μm diameter C_{18} packing (Waters Associates, Inc., Milford, MA).

Fluorescence detection of SA was accomplished with an F-1050 Hitachi fluorescence spectrophotometer (Hitachi Instruments, Inc., Danbury, CT) at an excitation wavelength of 305 $\pm$ 7.5 nm and an emission wavelength of 410 $\pm$ 7.5 nm. The pHBA was quantified at 250 nm and mHBA at 300 nm using a Shimadzu SPD-10AV absorbance detector (Shimadzu Scientific Instruments, Inc., Columbia, MD). Peak areas (SA) and heights (pHBA and mHBA) were determined using ELAB integration software (OMS Tech, Inc., Miami, FL).

For the nitrate actinometer, HPLC analyses were performed isocratically at a flow rate of 1.2 mL min^{-1} using a 0.2 μm-filtered 45/55% vol/vol methanol/25 mM phosphate buffer mobile phase. The phosphate-buffered aqueous phase was prepared by combining a 25 mM phosphoric acid solution with a 25 mM potassium phosphate (monobasic) solution to a pH of 2.1. For the nitrite actinometer, a solvent program was employed due to the coelution of a contaminant peak with the pHBA. Separations were performed for 3.6 min at 22/78% vol/vol methanol/25 mM phosphate buffer (pH 2.1) followed by 5 min at 75/25% methanol/25 mM phosphate buffer. The column was then re-equilibrated for 10 min at the initial 22/78% mobile phase composition. All HPLC analyses were performed shortly after an irradiation with time provided only for room temperature equilibration.

Analyte quantification. Salicylic acid and mHBA and pHBA were quantified by HPLC employing fluorescence and absorbance detection, respectively. A stock solution containing 20 μM SA, mHBA and pHBA was prepared in the actinometer solution previously described. Calibration curves were generated by standard additions of the stock solution to the actinometer solution, with final concentrations ranging from 10 to 1000 nM. This method of quantification yielded a coefficient of variation of 0.54% for SA and 0.64% for pHBA from multiple injections (n = 5) of a 500 nM standard; injection of a 50 nM standard yielded a coefficient of variation (n = 5) of 4.5% for SA and 7.1% for pHBA. The detection limit of this method, with a signal-to-noise ratio of two, was typically 0.6 nM for SA and 5 nM for pHBA. Detection limits were primarily dependent on the purity of the BA.

Molar absorption coefficients of nitrate and nitrite were determined in a 2.5 mM sodium bicarbonate solution containing 1 mM BA and either 10 mM sodium nitrate or 1 mM sodium nitrite. The

nitrate concentration was increased to 100 m*M* for absorption measurements made above 330 nm, while nitrite was increased to 10 m*M* for measurements above 400 nm. All absorbance measurements were made in a 10 cm quartz cell using a Hewlett Packard UV–visible spectrophotometer (model HP 8453). Absorption measurements were referenced against a pH 7.2, 2.5 m*M* sodium bicarbonate solution containing 1 m*M* BA. The molar absorption coefficient of SA was determined in a solution containing 10 μ*M* SA and 2.5 m*M* NaHCO$_3$, referenced against a 2.5 m*M* sodium bicarbonate solution.

Concentrations of nitrate were determined in the nitrate actinometer solution at 302 nm by Beer's law using the experimentally determined molar absorption coefficient value of 7.14 *M*$^{-1}$ cm^{-1}. The nitrite concentration was determined in the nitrite actinometer solution at 354 nm using a molar absorption coefficient value of 22.7 *M*$^{-1}$ cm^{-1}. For the determination of nitrate and nitrite concentrations, absorbances were referenced against a pH 7.2 solution of 1 m*M* BA and 2.5 m*M* sodium bicarbonate.

Batch fluorometry. Salicylic acid can be quantified by batch fluorescence without HPLC analysis. Batch quantification was performed using an ISS PC1 photon-counting spectrofluorometer (Champaign, IL). As with HPLC analysis, calibration curves were generated by standard additions of the stock solution to the actinometer solutions, with final concentrations ranging from 10 to 1000 n*M*. The response of the instrument was determined from the fluorescence of standards using 305 ± 2 nm excitation and 410 ± 2 nm emission.

Photochemical experiments. The irradiation system consisted of a 1 kW xenon lamp, a GM 252 high intensity quarter meter grating monochromater and an enclosed sample chamber (Spectral Energy Corp., Westwood, NJ). A 2.5 nm bandwidth was used for all photolyses, with the exception of nitrate irradiations at wavelengths >335 nm and nitrite irradiations at wavelengths >400 nm, where a 5.0 nm bandwidth was selected due to the low molar absorption coefficients of nitrate and nitrite, respectively.

For all irradiations, a 3.1 mL aliquot of the nitrate or nitrite solution was placed in a 1 cm quartz cell with a screw cap containing a Teflon septum. The solution was equilibrated in the dark to the selected temperature for at least 20 min. The sample chamber temperature was controlled with a Fisher Scientific circulating water bath (model 9005). The sample was continually stirred throughout the irradiation. To eliminate condensation on the quartz cell at low temperatures, the sample chamber was dehumidified with a stream of dry air that was obtained by passing compressed air through a packed column containing Drierite (Fisher Scientific). Irradiation times ranged from 10 to 20 min, except for wavelengths >330 nm for nitrate irradiations and >380 nm for nitrite irradiations where samples were irradiated from 1 to 2 h. Controls were irradiated from 10 min to 2 h, depending on the wavelength. For these controls, an aluminum foil plate was placed in front of the light inlet of the sample chamber. All samples were allowed to equilibrate to room temperature and subsequently analyzed for SA and pHBA production by HPLC.

Actinometry. Radiant fluxes were determined at each wavelength using the chemical actinometer potassium ferrioxalate (1). A solution of 8.7 m*M* potassium ferrioxalate in 0.05 *M* sulfuric acid was used for all wavelengths. For each wavelength, a 3.1 mL aliquot of the actinometer solution was irradiated for 3 min. After the ferrioxalate solution was irradiated, it was transferred in the dark to a red-illuminated room. Subsequently, 0.5 mL of a buffer (pH 4.55) containing sodium acetate (0.60 *M*) and sulfuric acid (0.18 *M*), 2.0 mL of 0.2% wt/wt 1,10-phenanthroline aqueous solution and 6.5 mL of Milli Q water were added to a 1 mL aliquot of the irradiated sample (28). Blanks were prepared using nonirradiated samples. Samples were reacted for 45 min at room temperature. Absorbance measurements were made in a 1 cm quartz cell at 510 nm with a Spectronic Genesys absorbance detector (Spectronic Instruments, Rochester, NY). All samples were analyzed in duplicate. The radiant flux, E (einstein min^{-1}), was then calculated using the actinometry equation described in Kuhn *et al.* (28), with inclusion of a cell pathlength term in the denominator:

$$E = \frac{10^{-3}AV_2V_3}{\epsilon \Phi V_1 tl} \tag{5}$$

where A is the absorbance of the ferrous-complexed solution at 510

nm, V$_1$ is the volume of the irradiated solution (1.0 mL), V$_2$ is the volume of the PFA irradiated (3.1 mL), V$_3$ is the volume of the complexed solution (10 mL), ϵ is the molar absorption coefficient of the ferrous phenanthroline complex at 510 nm, t is the irradiation time and l is the pathlength of the cell used for the absorbance measurement.

The valerophenone actinometer was prepared at a concentration of 5 × 10^{-6} *M* valerophenone in water containing 0.05% acetonitrile (vol/vol). This solution was prepared from a 0.010 *M* stock solution of valerophenone in acetonitrile as described in Zepp *et al.* (2). Valerophenone concentrations were determined using HPLC with absorbance detection at 250 nm. The HPLC analyses were performed isocratically at a flow rate of 1.2 mL min^{-1} using a 30/70% (vol/vol) water/acetonitrile mobile phase. The HPLC column was the same as that described for SA and pHBA separations (*vide supra*). A standard curve was generated with concentrations ranging from 1 to 5 μ*M* valerophenone in water with 0.05% acetonitrile (vol/vol).

Quantum yield determinations. Quantum yields for SA and pHBA production were determined in air-saturated solutions at 5 nm intervals from 290 to 350 nm for nitrate photolysis and at 10 nm intervals from 290 to 405 nm for nitrite photolysis. The equation used to determine the quantum yield for SA or pHBA production at a given wavelength (λ) under optically thin conditions is

$$\Phi_\lambda = \frac{[X]V}{2.303E_\lambda \epsilon_\lambda lt[NO_x^-]} \tag{6}$$

where [X] is the pHBA or SA concentration produced during an irradiation (*M*), V is the volume of the irradiated solution (L), E is the radiant flux (determined by ferrioxalate actinometry) (einstein min^{-1}), ϵ is the molar absorption coefficient of nitrate or nitrite at the selected wavelength (*M*$^{-1}$ cm^{-1}), l is the pathlength of the irradiation cell (cm), t is the irradiation time (min) and [NO$_x^-$] is the concentration of nitrate or nitrite in the irradiated solution (*M*). The radiant flux in the 1 cm quartz cell varied from 1.0 to 4.0 × 10^{-7} einstein min^{-1} over the wavelength range considered, as determined by PFA. For all quantum yield determinations, initial rate conditions were maintained with no loss of nitrate or nitrite observed during irradiations as determined by spectrophotometry.

Temperature dependence. The temperature dependence of the quantum yields for SA or pHBA production was determined at 5 nm intervals for the nitrate actinometer and at 20 nm intervals for the nitrite actinometer. For nitrate, the temperature dependence was determined from 290 to 330 nm, while for nitrite, the temperature dependence was determined from 310 to 390 nm. For each wavelength band examined, quantum yields were determined at 5, 15, 25 and 35°C. Nonlinear Arrhenius plots of the quantum yield *versus* reciprocal temperature were generated to determine the activation energy (E$_a$) for each wavelength using nonlinear least-squares regression analysis.

Determination of actinometer response as a function of time and intensity. Experiments were conducted to demonstrate that the production of SA and pHBA in the actinometers was dependent on the photon flux only, and not on the radiant intensity or time of irradiation (*i.e.* the condition of reciprocity was met). To demonstrate linearity of response with time, the actinometers were irradiated at 310 nm and 25°C for 1–120 min. The response of the actinometers was then plotted as a function of time.

To demonstrate that the quantum yields for SA and pHBA production were independent of radiant intensity, a series of screens and neutral density filters were employed. By varying the combinations of screens and filters, irradiations at 310 nm were conducted at radiant intensities ranging from 36.5 to 380 × 10^{-12} einsteins s^{-1} as determined by PFA. Salicyclic acid and pHBA production were then plotted as a function of the radiant intensity.

Determination of percentage of OH reacting with BA. The relative proportion of photochemically produced OH reacting with BA was determined in the 10 m*M* nitrate actinometer solution that was irradiated for 15 min at 305 nm and 25°C. Solutions were prepared with BA concentrations ranging from 1 to 1000 μ*M*. The pH of these solutions ranged from 7.2 to 8.2. A plot of production rate of the products (SA and pHBA) *versus* BA concentration was generated to demonstrate saturation for the nitrate actinometer. Complete scavenging of the OH radical was expected based on published sec-
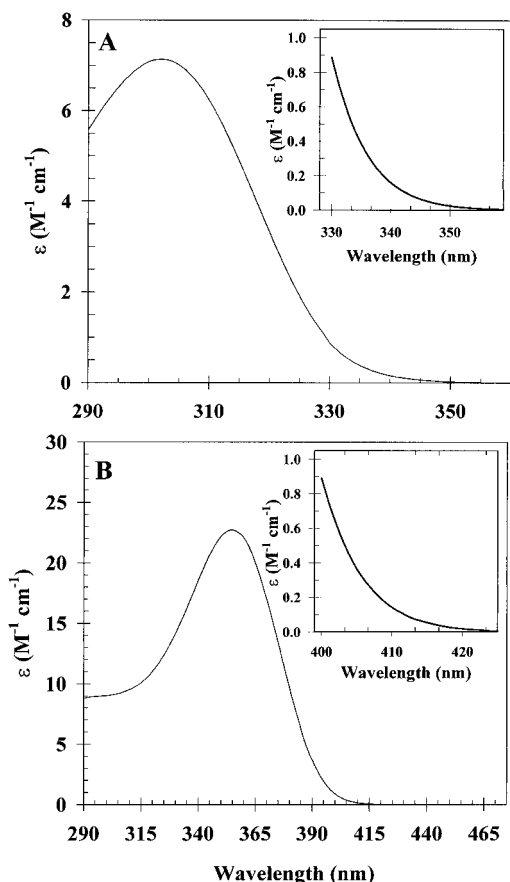
Figure 1. The molar absorption coefficient (ϵ) plotted as a function of wavelength for (A) 10 m*M* nitrate and (B) 1 m*M* nitrite in a 2.5 m*M* bicarbonate solution containing 1 m*M* BA. The inset in panel A is a plot of ϵ_{NO3-} *versus* wavelength from 330 to 360 nm for 100 m*M* nitrate. The inset in panel B is a plot of ϵ_{NO2-} *versus* wavelength from 400 to 425 nm for 10 m*M* nitrite. All spectra were referenced against a 2.5 m*M* bicarbonate/1 m*M* BA solution (pH 7.2).

ond-order rate constants for the reaction of the OH radical with BA, nitrate and the bicarbonate ion.

In the nitrite actinometer solution, a large fraction of the OH radical was expected to react with the nitrite ion based on the large value of its second-order rate constant (1.1×10^{10} M^{-1} s^{-1}) (29). Because of this high rate constant and the limited solubility of BA in water, complete scavenging of the OH radical was not achieved. Therefore, literature values for the second-order rate constants for the reaction of OH with BA, nitrite and bicarbonate ion were used to estimate the percentage of OH that reacts with BA in the 1 m*M* nitrite actinometer.

RESULTS

Absorption spectra

Molar absorption coefficients were determined for nitrate from 290 to 360 nm and for nitrite from 290 to 425 nm. The molar absorption coefficient of nitrate is plotted as a function of wavelength in Fig. 1A. Based on this plot, nitrate absorbs primarily from 290 to 330 nm, with a maximum absorption at 302 nm. Nitrite absorption occurs throughout the UVB and UVA, with a maximum absorption at 354 nm (Fig. 1B). Molar absorption coefficient values reported here are in excellent agreement with published values for both nitrate (*e.g.* ϵ_{305} = 7.01 *vs* 6.93 M^{-1} cm^{-1} [30]) and nitrite (*e.g.* ϵ_{354} =
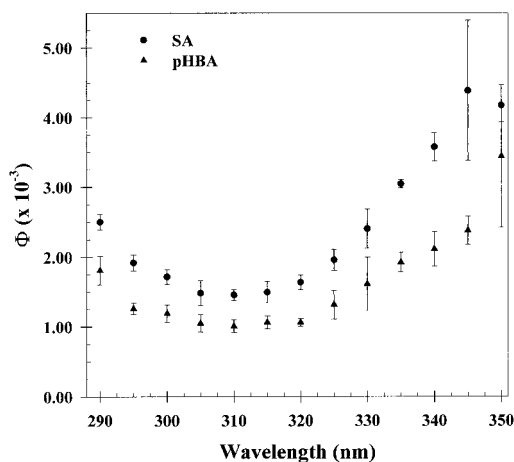

Figure 2. The wavelength-dependent quantum yield for SA and pHBA production from the photolysis of 10 m*M* nitrate in the actinometer solution. Error bars denote the 95% confidence interval (n = 3–12).

22.73 *vs* 22.93 M^{-1} cm^{-1} [31]). Our results extend molar absorption coefficient values to longer wavelengths, as previous values were reported only to 335 nm for nitrate (30) and 400 nm for nitrite (31).

Tabulated data for the nitrate and nitrite molar absorption coefficients and quantum yields for SA and pHBA production (*vide infra*) are presented in: Jankowski, J. J. The Development and Application of Ultraviolet Solar Actinometers. Ph.D. Thesis. SUNY Environmental Science and Forestry, Syracuse, NY (1999).

SA and pHBA quantum yields from nitrate photolysis

Quantum yields for the production of SA and pHBA from nitrate photolysis were determined in air-saturated solutions from 290 to 350 nm at 25°C, as shown in Fig. 2. The quantum yields reported here are based on initial rate conditions, with no loss of nitrate or BA observed. No production of SA or pHBA was observed in dark controls. Quantum yields for SA and pHBA production from nitrate photolysis showed the same wavelength dependence; however, the quantum yield for SA formation was approximately 50% greater than that for pHBA formation at all wavelengths. The SA quantum yield decreased from 0.00250 at 290 nm to 0.00149 at 305 nm, while the pHBA quantum yield decreased from 0.00181 at 290 nm to 0.00105 at 305 nm. Quantum yields for SA and pHBA production remained nearly constant (95% confidence interval [CI]) from 305 nm to 320 nm at 0.00152 ($\pm$0.00004) for SA production (n = 49) and 0.00105 ($\pm$0.00003) for pHBA production (n = 42). Above 320 nm, quantum yields increased with increasing wavelength for the production of both SA (from 0.00164 at 320 nm to 0.00418 at 350 nm) and pHBA (from 0.00106 at 320 nm to 0.00345 at 350 nm) (Fig. 2).

The higher quantum yields observed at the longer wavelengths are not an artifact of the photolysis of nitrite. Nitrite interference was considered because the photolysis of nitrite is a source of the hydroxyl radical (18) and because nitrite reacts with the OH radical. Nitrite is produced from the photolysis of nitrate (reaction 2) and may exist as a contaminant
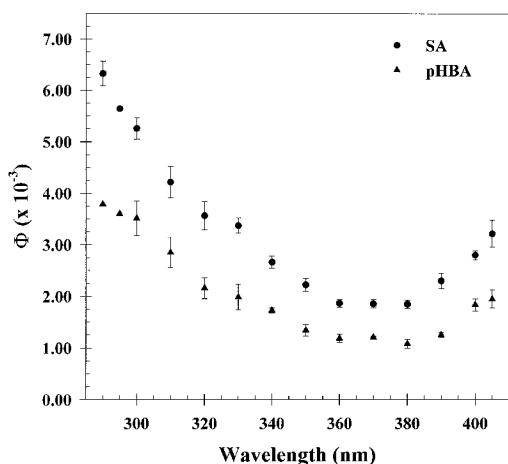
Figure 3. The wavelength-dependent quantum yield for SA and pHBA production from the photolysis of 1 mM nitrite in the actinometer solution. Error bars denote the 95% CI (n = 4–14).

Figure 4. Natural logarithm of the 320 nm quantum yields for SA and pHBA production from the photolysis of nitrate plotted as a function of the reciprocal temperature (K^{-1}). The best-fit line through the data was determined by linear regression analysis. The coefficient of determination (r^2) and the slope (95% CI) were 0.931 and -1.59 ± 0.26 K for SA and 0.949 and -2.13 ± 0.30 K for pHBA.

in the nitrate solution. No nitrite contamination was detected in nonirradiated nitrate solutions as determined by standard flow-injection colorimetric analysis (32) (detection limit ~0.05 μM), and less than 100 nM nitrite was formed during nitrate irradiations because initial rate conditions were maintained. At these nitrite concentrations and concentrations up to 1 μM, nitrite did not affect the trapping efficiency of the OH radical by BA (Jankowski *et al.,* unpublished results). This was expected, because based on the published second-order rate constants for the hydroxyl radical with nitrite (1.1 $\times$ 10^{10} M^{-1} s^{-1}) (29) and BA (5.9 $\times$ 10^9 M^{-1} s^{-1}) (33), the rate of reaction of 1 mM BA with OH is approximately 500 times greater than the reaction of 1 μM nitrite with the OH radical.

SA and pHBA quantum yields from nitrite photolysis

Quantum yields for SA and pHBA production from the photolysis of 1 mM nitrite in air-saturated solutions were determined from 290 to 405 nm at 25°C employing initial rate conditions. A plot of the quantum yield for SA and pHBA production *versus* wavelength is shown in Fig. 3. The quantum yields for SA and pHBA production showed the same wavelength dependence, with the quantum yield for SA production approximately 60% greater than the quantum yield for pHBA production at all wavelengths. Quantum yields decreased by more than a factor of three from 0.00633 for SA production and 0.00379 for pHBA production at 290 nm to 0.00187 for SA and 0.00118 for pHBA at 360 nm. From 360 nm to 380 nm, the quantum yields for SA and pHBA production were constant (95% CI) with a value of 0.00187 $\pm$ 0.00004 for SA and 0.00116 $\pm$ 0.00005 for pHBA (n = 14). Above 380 nm, quantum yields increased from 0.00185 for SA and 0.00108 for pHBA at 380 nm to 0.00322 for SA and 0.00195 for pHBA at 405 nm.

Activation energy

The temperature dependence of the quantum yield for SA and pHBA production from nitrate photolysis followed Arrhenius theory for all wavelengths considered, as previously observed for hydroxyl radical production at 308 nm (13). An
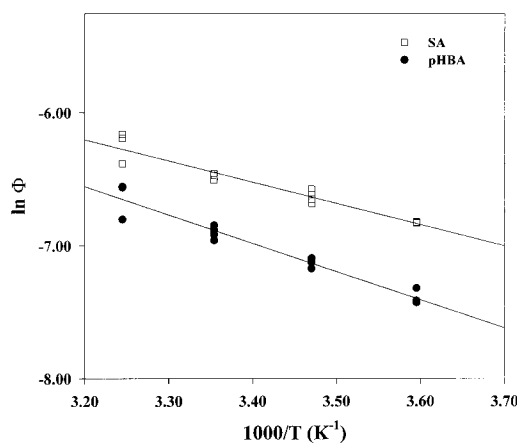
example is shown in Fig. 4, which depicts the Arrhenius plot for SA and pHBA production from nitrate photolysis at 320 nm. Activation energies for SA and pHBA production (99% CI) were generated from nonlinear regression analysis of the plot of quantum yield *versus* temperature. The wavelength-dependent activation energy is a composite activation energy that reflects the effect of temperature on the primary photochemical process, the addition of the OH radical to the ring and the subsequent decay of the radical to produce the product (SA or pHBA). For all wavelengths examined, higher activation energies were found for pHBA production than for SA production (Table 1). For both SA and pHBA formation, the minimum activation energy was found at 290 nm (SA = 14.7 kJ mol^{-1}; pHBA = 15.0 kJ mol^{-1}). The activation energy between 295 and 325 nm showed little change with respect to wavelength for both SA and pHBA. In this region, the mean average activation energy for SA formation was 16.0 kJ mol^{-1}, ranging from 15.6 kJ mol^{-1} (at 325 nm) to 16.5 kJ mol^{-1} (at 305 nm). The mean activation energy for pHBA in this region was approximately 17.0 kJ mol^{-1}, with a minimum value of 16.7 kJ mol^{-1} (300 nm) and a maximum of 17.2 kJ mol^{-1} (310 nm). A slight

Table 1. The wavelength-dependent activation energy for SA and pHBA production in the 10 mM nitrate actinometer, as determined by nonlinear regression analysis*

Wavelength (nm)	SA E$_A$ (kJ mol^{-1})	pHBA E$_A$ (kJ mol^{-1})
290	14.7 $\pm$ 0.2	15.0 $\pm$ 0.2
295	15.6 $\pm$ 0.2	17.1 $\pm$ 0.2
300	15.9 $\pm$ 0.2	16.7 $\pm$ 0.5
305	16.5 $\pm$ 0.1	16.8 $\pm$ 0.1
310	16.3 $\pm$ 0.1	17.2 $\pm$ 0.2
315	16.2 $\pm$ 0.2	17.1 $\pm$ 0.1
320	15.9 $\pm$ 0.1	17.0 $\pm$ 0.1
325	15.6 $\pm$ 0.1	16.8 $\pm$ 0.1
330	14.9 $\pm$ 0.1	15.7 $\pm$ 0.6

*Error bars denote the 99% CI.

Table 2. The wavelength-dependent activation energy for SA and pHBA production in the 1mM nitrate actinometer, as determined by nonlinear regression analysis*

Wavelength (nm)	SA E_A (kJ mol^{-1})	pHBA E_A (kJ mol^{-1})
310	12.3 ± 0.7	13.6 ± 0.7
330	12.9 ± 0.6	14.3 ± 0.5
350	13.9 ± 1.0	15.3 ± 0.9
370	14.6 ± 0.8	15.7 ± 0.8
390	17.8 ± 0.9	19.3 ± 0.9

*Error bars denote 99% CI.

decrease in activation energy was observed for both SA and pHBA at 330 nm relative to the 295–325 nm range (SA = 14.9 kJ mol^{-1}; pHBA = 15.7 kJ mol^{-1}). The lower activation energies reported for both SA and pHBA production at 290 nm and 330 nm are significantly different at the 99% confidence level from the higher activation energy determined at 310 nm, as determined by a two-tailed F-test at an α level of 0.001.

Composite activation energies for SA and pHBA production from nitrite photolysis were determined at 20 nm intervals from 310 to 390 nm. As with nitrate photolysis, SA and pHBA production from nitrite photolysis followed Arrhenius theory at all wavelengths. The activation energy for SA and pHBA production from nitrite photolysis was determined by nonlinear regression analysis. As shown in Table 2, the activation energy (99% CI) increased with wavelength from 12.3 ± 0.7 kJ mol^{-1} for SA production and 13.6 ± 0.7 kJ mol^{-1} for pHBA production at 310 nm to 17.8 ± 0.9 kJ mol^{-1} for SA and 19.3 ± 0.9 kJ mol^{-1} at 390 nm.

Although statistical differences were observed, changes in activation energies with respect to wavelength were small. Over the wavelength region examined, the range in activation energy was 1.8 and 2.2 kJ mol^{-1} for SA and pHBA production from nitrate photolysis, respectively, and 5.5 and 5.7 kJ mol^{-1} for SA and pHBA production from nitrite photolysis.

The temperature-dependent quantum yield (Φ) of the SA and pHBA production can be determined using the following equation:

$$\ln\frac{\Phi_{T1}}{\Phi_{T2}} = \frac{E_A}{R}\left(\frac{1}{T_2} - \frac{1}{T_1}\right) \tag{7}$$

where E_A is the activation energy and R is the universal gas constant. Using Eq. 7 and the mean activation energy for the wavelength range studied, quantum yields for SA and pHBA formation from nitrate photolysis will increase by factors of 2.2 and 2.3, respectively, for a temperature increase from 0 to 35°C. For nitrite photolysis from 0 to 35°C, the quantum yield will increase by a factor of 2.0 for SA production and 2.2 for pHBA production.

Actinometer response as a function of time and intensity

The production of SA and pHBA was determined at varying radiant light fluxes and radiant intensities in order to demonstrate reciprocity. The photochemical production of SA and pHBA at 330 nm and 25°C in the nitrate and nitrite actinom-
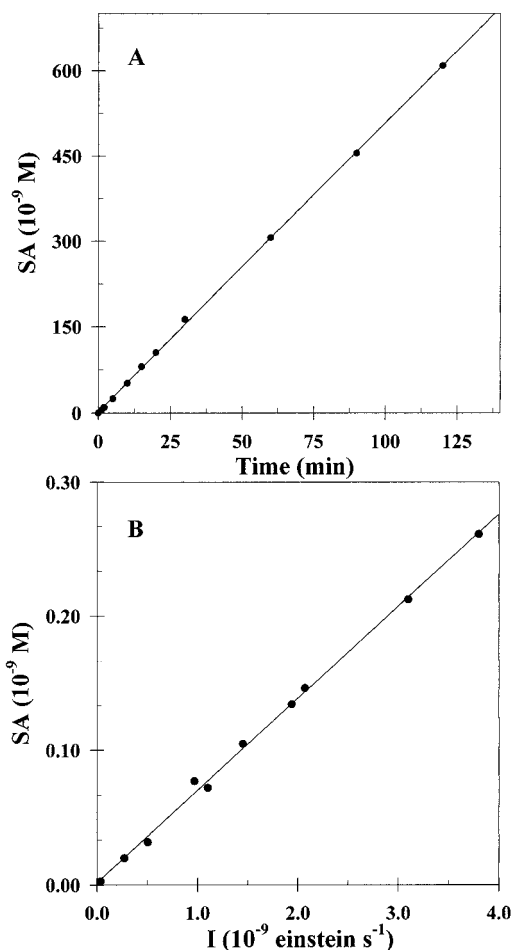

Figure 5. (A) The production of SA from nitrate photolyis in air-saturated solutions at 330 nm and 25°C *versus* time at a constant radiant intensity of 5.15×10^{-9} einstein s^{-1}. The best-fit line through the data was determined by linear regression analysis. The coefficient of determination (r^2) was 1.00 and the slope (95% CI) was 5.06 ± 0.06 × 10^{-9} M min^{-1}. (B) The SA production in the nitrate actinometer at 310 nm and 25°C as a function of radiant intensity, as determined by PFA. The best-fit line through the data was determined by linear regression analysis. The coefficient of determination (r^2) was 0.997 and the slope (95% CI) was 0.069 ± 0.003 M s einstein^{-1}.

eters was a linear function of the radiant flux for irradiations ranging from 1 to 120 min at a constant radiant intensity (5.15 × 10^{-9} einsteins s^{-1}). Linear regression analysis of analyte production *versus* time yielded excellent correlations, with r^2 values >0.99 determined for SA and pHBA production (n = 10) in both the nitrate (Fig. 5A) and nitrite actinometers (data not shown). Additionally, the radiant fluxes determined from the respective linear regression analyses agreed within 5% of the values determined by PFA actinometry.

Production of SA and pHBA in the nitrate actinometer increased linearly with respect to the radiant intensity over two orders of magnitude, as determined by PFA, with irradiances varying from 36.5 to 380 × 10^{-12} einsteins s^{-1} (Fig. 5B). Production in the nitrite actinometer was also a linear function of intensity over two orders of magnitude (data not shown). Linear regression analysis of these plots also yielded excellent correlations, with r^2 values >0.99 observed for SA and pHBA production (n = 10) in the nitrate and nitrite
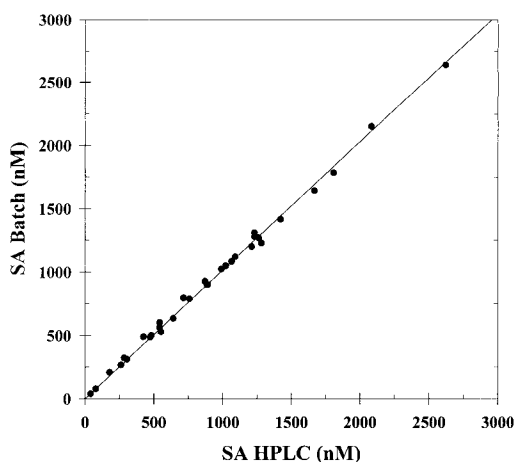
Figure 6. The concentration of SA in the nitrate actinometer as determined by batch fluorescence using an ISS scanning fluorometer *versus* the concentration determined using HPLC analysis with fluorescence detection. The best-fit line through the data was determined by linear regression analysis. The coefficient of determination (r^2) was 0.998 and the slope (95% CI) was 1.02 ± 0.02.

actinometers. These results indicate that corresponding quantum yields for SA and pHBA production were constant and independent of the radiant intensity employed.

Batch fluorometry

To demonstrate that batch fluorescence was a suitable method of analysis for irradiated samples, the SA concentration in the irradiated nitrate actinometer determined by the ISS fluorometer was compared to the SA concentration determined by the HPLC method (Fig. 6). Excellent agreement was shown between the two methods for SA production ranging from 40 to 2600 nM, as determined by linear regression analysis (slope [95% CI] = 1.02 ± 0.02; r^2 = 0.998).

Trapping efficiency of OH by BA

The trapping efficiency of OH by BA was quantified to estimate quantum yields for the production of the OH radical from nitrate photolysis (*vide infra*). The benzoate ion is an efficient scavenger of the hydroxyl radical ($k = 5.9 \times 10^9$ L mol^{-1} s^{-1} [33]) and has been used as a probe for OH in aqueous systems (21,27). However, the bicarbonate ion and nitrate ions are also known to react with the hydroxyl radical, with reported second-order rate constants of 8.5×10^6 L mol^{-1} s^{-1} (33) and $<5 \times 10^5$ L mol^{-1} s^{-1} (34), respectively. To determine the efficiency of OH radical scavenging by BA in the nitrate actinometer, a study was conducted to determine the effect of BA concentration on the formation of SA and pHBA. A plot of the rate of formation of SA or pHBA at 305 nm *versus* BA concentration is shown in Fig. 7. At a concentration of 1 mM in the nitrate actinometer solution, BA scavenges virtually all of the OH formed. This is in agreement with the predicted value of 99.6% of OH reacting with BA in the nitrate actinometer estimated from the literature rate constants for BA, nitrate and the bicarbonate ion.

For the nitrite actinometer, it was not possible to achieve complete scavenging of the OH radical because of BA sol-
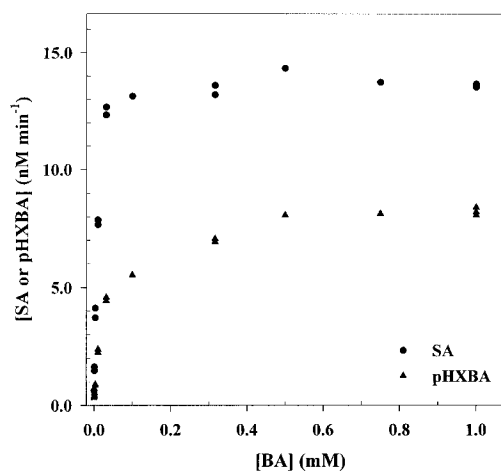

Figure 7. Plot of the SA and pHBA production rate at 305 nm and 25°C as a function of BA concentration in the nitrate actinometer.

ubility limitations. Thus, literature values were used to estimate the relative percentage of OH reacting with 1 mM nitrite and BA. Based on the literature values of the second-order rate constants for the reaction of OH with BA and nitrite, 5.9×10^9 (33) and 1.1×10^{10} L mol^{-1} s^{-1} (29), respectively, and the concentrations of these species in the nitrite actinometer solution (1 mM), BA reacts with 35% of the OH radicals produced during the photolysis of the nitrite actinometer.

DISCUSSION

Nitrate and nitrite are well suited actinometers for the measurement of monochromatic radiant fluxes. Because of the low quantum yields for nitrate and nitrite photolysis, initial rate conditions can be maintained for hours. The production of SA and pHBA in both the nitrate and nitrite actinometers is linear over several orders of magnitude with respect to both time and intensity. The nitrate and nitrite actinometers have advantages over currently used actinometers in both their sensitivity and their ease of use. Because the actinometers quantify light based on the formation of a product, they are inherently more sensitive than actinometers that are based on loss of a chromophore. For example, during a 1 min irradiation with a radiant flux of 3×10^{-7} einstein min^{-1} at 313 nm, 18 nM and 9 nM SA will be produced at 25°C in the nitrate and nitrite actinometers, respectively. This corresponds to signals approximately 30 and 15 times greater than the detection limit for SA. By comparison, under the same irradiation conditions (3 mL actinometer, 1 cm pathlength), irradiation of the PNA/pyridine (pyr) actinometer (3) will result in approximately a 1% change in PNA concentration, to be quantified by absorption detection ([pyr] = 12.4 mM; $\epsilon_{PNA} = 1.0 \times 10^4 M^{-1}$ cm^{-1}; $\Phi_{PNA} = 5.7 \times 10^{-3}$).

Potassium ferrioxalate actinometry, also based on production of a chromophore, is as sensitive as the nitrate and nitrite actinometers but is inferior in terms of ease of use. Because the nitrate and nitrite actinometers are insensitive to standard laboratory lighting, no darkroom is needed. When batch fluorescence is chosen for SA analysis, the nitrate/nitrite actinometers have a much simpler detection method than PFA, which requires complexation of the pho-
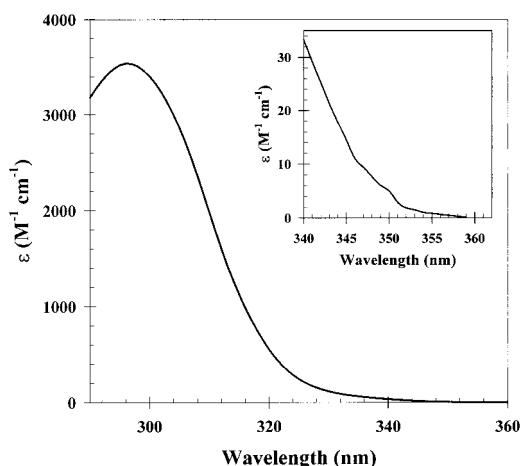
Figure 8. The molar absorption coefficient (ϵ) of 10 μM SA plotted as a function of wavelength in a 2.5 mM bicarbonate solution (pH 8.2). The inset is a plot of ϵ_{SA} *versus* wavelength from 340 to 360 nm for 100 mM SA. Both spectra were referenced against a 2.5 mM bicarbonate solution.

tochemically produced ferrous iron. Finally, the nitrate and nitrite actinometer solutions are quite stable under refrigeration both prior to and after irradiation. Salicylic acid was stable in the filtered, irradiated actinometer solution for at least 6 weeks when refrigerated. The pHBA in the actinometer solutions also demonstrated stability under refrigeration, but can be prone to bacterial degradation if not prepared using high purity water. In bacteria-free water, irradiated samples can be refrigerated and analyzed at a later time and not necessarily in the laboratory where the light measurements were made. This is contrasted by PFA actinometry that requires prompt analysis of the complexed iron to avoid reoxidation of the ferrous iron, as well as daily preparation of the phenanthroline complex.

With the determination of the wavelength and temperature dependence of the quantum yields for SA and pHBA production, Eq. 6 can be used to determine the radiant flux, E. When the radiant flux is integrated with respect to time, the minimum radiant energies that can be detected in our irradiation system are approximately 10^{-9} and 10^{-8} einsteins, based on the detection limits for SA and pHBA (*vide supra*), respectively.

Salicylic acid absorbs UV light at wavelengths <360 nm (Fig. 8). In this region, photochemical degradation of SA occurs with a wavelength-independent quantum yield of approximately 0.012 (Jankowski *et al.,* manuscript submitted). For a 310 nm irradiation of the nitrate actinometer (3.1 mL, 1 cm pathlength) with a radiant intensity of 5.07×10^{-9} einstein s^{-1}, the first-order rate constant for SA degradation is 8.96×10^{-5} s^{-1}, while the corresponding pseudofirst-order rate constant for SA production is 3.57×10^{-8} s^{-1}. Based on these rate constants, a 10 mM nitrate actinometer solution containing 50 nM SA will produce SA at a rate 80 times greater than SA degradation; this provides a 99% actinometer response relative to initial conditions. Thus, degradation of SA was not taken into account for the quantum yield studies presented here (maximum SA production = 81 nM at 310 nm). Additionally, SA production was linear with time over a 2 h irradiation at 330 nm (Fig. 5A). However,

photolysis of SA may need to be considered for very long-term irradiations at wavelengths below approximately 345 nm. Under these conditions, radiant fluxes can be determined from the formation of pHBA because its rate constant for photolysis is approximately two orders of magnitude lower than SA (Jankowski *et al.,* manuscript submitted).

Multiple electronic transitions

There is a debate in the literature regarding the electronic transition of the nitrate absorption band centered at 302 nm (5–8,35). The possibility of multiple electronic transitions has been suggested (5,10) and this may explain the differences that have been noted on whether absorption in this region can be attributed to an n $\rightarrow$ σ^* (7,8) or n $\rightarrow$ π^* transition (6,35). The changes in quantum yields for SA and pHBA production from nitrate photolysis below 305 nm and above 320 nm (Fig. 2) are evidence for an overlap of electronic transitions of nitrate in this wavelength band. Overlap of the stronger absorbing $\pi \rightarrow \pi^*$ band (4) of nitrate (centered at 201 nm) with the weaker absorbing band(s) (centered at 302 nm) may account for the decrease in quantum yield seen from 290 to 305 nm. Further evidence of a change in electronic transition includes the lower activation energies for SA and pHBA production found at 290 and 330 nm relative to the activation energies determined from 295 nm to 325 nm (Table 1). We hypothesize that changes in the electron transition of nitrate may result in a change in the relative importance of hydroxyl radical formation *versus* atomic oxygen formation (reactions 1 and 2) as a function of wavelength. This change in branching ratio with wavelength may be directly responsible for the observed quantum yield changes presented here, although this was not examined.

To demonstrate that the increase in quantum yields for SA and pHBA production with respect to wavelength above 320 nm was not an analytical artifact, an intercomparison of the nitrate actinometer with the published valerophenone actinometer (2) was conducted at 330 nm. Irradiations were performed in air-saturated solutions at 25°C for 5 to 25 min (n = 6). For valerophenone, the radiant flux, E, was calculated using the following equation:

$$E = \frac{k}{2.303(\epsilon)(\Phi)(l/v)} \qquad (8)$$

where k is the slope of the plot of the natural log of valerophenone concentration *versus* time (determined by linear regression analysis (Fig. 9A)), ϵ is the molar absorption coefficient for valerophenone, Φ is the quantum yield for valerophenone photolysis and l/v is the pathlength to volume ratio of the valerophenone solution in the quartz cuvette (2). For the nitrate actinometer, the radiant flux was determined from linear regression analysis of SA production *versus* time using Eq. 6 (Fig. 9B). The radiant fluxes (95% CI) determined by the two methods were in excellent agreement, with valerophenone yielding a value of 0.313 ($\pm$0.075) μeinstein min^{-1} compared to 0.301 ($\pm$0.015) μeinstein min^{-1} using the nitrate actinometer and 0.306 ($\pm$0.015) μeinstein min^{-1} using the nitrite actinometer (data not shown).

As with nitrate, the presence of multiple electronic transitions is suggested for nitrite based on changes in the quan-
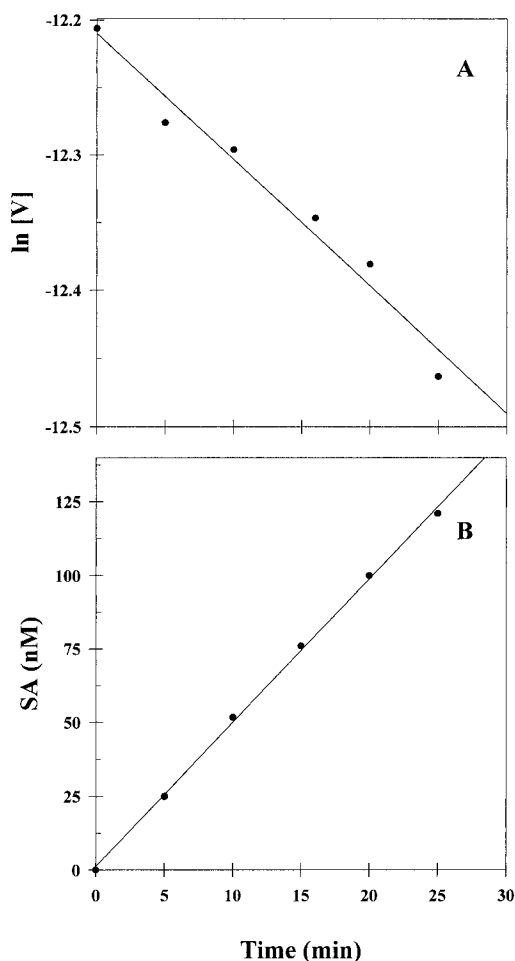
Figure 9. (A) Plot of the natural log of valerophenone concentration *versus* time during irradiation at 330 nm and 25°C. The best-fit line through the data was determined by linear regression analysis. The coefficient of determination (r^2) was 0.970 and the slope (95% CI) was -0.00934 ± 0.00232 min^{-1}. (B) The production of SA in the nitrate actinometer at 330 nm and 25°C *versus* time. The best-fit line through the data was determined by linear regression analysis. The coefficient of determination (r^2) was 0.999 and the slope (95% CI) was 4.89 ± 0.25 nM min^{-1}.

Table 3. Quantum yields for OH radical production from nitrate photolysis at 25°C estimated from SA and pHBA production in the nitrate actinometer compared to previously reported values*

λ (nm)	NO_3^- Φ_{OH} from Φ_{SA}	NO_3^- Φ_{OH} from Φ_{pHBA}	NO_3^- Φ_{OH} published
290	0.009	0.011	0.010 (37)
295	0.009	0.009	0.011 (37)
300	0.008	0.008	0.009 (37)
305	0.007	0.007	0.0092 (14)
308	0.007	0.007	0.017 (13)
313	0.007	0.007	0.013 (12)
			(at 20°C)
320	0.008	0.007	
330	0.012	0.014	

*All published values are at 25°C, unless otherwise denoted.

the speciation and concentrations of metals and organic compounds. The primary source of the OH radical in natural waters is through the photolysis of nitrate, nitrite and dissolved organic matter (27,36,37). Although the production of the OH radical from nitrate photolysis has been the topic of numerous studies, the wavelength dependence of OH radical production from nitrate photolysis has not been determined. Wavelength-dependent quantum yields for OH production from nitrate photolysis were estimated from SA and pHBA quantum yields. We used our experimentally determined ratio of 1:1:0.6 for the *o:m:p*-monohydroxybenzoic acid production from nitrate photolysis at 25°C and Matthews and Sangster's (23) value of 0.56 to account for the fraction of non-hydroxylated products formed from the reaction of the OH radical with BA. Using these values, the SA quantum yield was multiplied by a factor of 4.6 and pHBA quantum yield by a factor of 7.7 to estimate the wavelength-dependent OH radical quantum yield for nitrate photolysis from 290 to 330 nm (Table 3). The OH radical quantum yields estimated from SA and pHBA quantum yields agree very well with values determined using initial rate conditions by Vaughan and Blough (37) at 290, 295 and 300 nm, and Warneck and Wurzinger (14) at 305 nm. Estimated values were approximately half the values reported by Zepp *et al.* (12) at 313 nm and Zellner *et al.* (13) at 308 nm. Differences in the reported quantum yields may be due to penetration of the solvent cage by the probe at high scavenger concentrations (~0.3 *M* [13]) that has been postulated to lead to higher quantum yields (14,15). Alternatively, the efficiency of the production of the hydroxybenzoic acids relative to the nonhydroxylated products that we assumed for the calculation of OH quantum yields may not be valid for the conditions of these experiments.

The wavelength-dependent production of the OH radical from nitrite photolysis can also be estimated from the SA and pHBA quantum yields presented here. Hydroxyl radical quantum yields for nitrite photolysis were estimated from 298 to 390 nm (Table 4) by employing a factor of 2.9 to account for nitrite scavenging of the OH radical (*vide supra*), in addition to the factors used to account for the *o:m:p* ratio and nonhydroxylated products (4.6 for SA and 7.7 for pHBA). Estimated OH radical quantum yield values are in good agreement with published values determined at 298 nm (19), 308 nm (13,37) and 354 nm (19,37). The estimated

tum yield for SA and pHBA production from nitrite photolysis below 360 nm and above 380 nm. The decrease in the quantum yield for SA production from nitrite photolysis with increasing wavelength in the region from 290 to 360 nm reflects a more efficient production of the OH radical in the lower wavelength n $\rightarrow$ π* transition band of nitrite, relative to the second n $\rightarrow$ π* transition. This is in agreement with previous nitrite quantum yield studies for OH formation (19) and is further supported by the increase in activation energy with increasing wavelength found for SA production from nitrite photolysis (Table 2). Overlap of the π $\rightarrow$ π* transition band (ϵ_{max} at 220 nm) into the lower wavelengths of the UVB has also been implicated (19) and may partly account for the decrease in quantum yield with increasing wavelength.

OH quantum yield estimates

The hydroxyl radical is the strongest and least selective oxidant that has been detected in natural waters, and it affects

Table 4. Quantum yields for OH radical production from nitrite photolysis at 25°C estimated from SA and pHBA production in the nitrate actinometer compared to previously reported values*

λ (nm)	NO$_2^-$ Φ$_{OH}$ from Φ$_{SA}$	NO$_2^-$ Φ$_{OH}$ from Φ$_{pHBA}$	NO$_2^-$ Φ$_{OH}$ published
298	0.070	0.078	0.07 (19)
308	0.057	0.065	0.062 (13)
			0.07 (37)
337	0.037	0.041	0.07 (19)
351	0.030	0.030	0.046 (13)
354	0.028	0.028	0.02 (19)
			0.029 (37)
371	0.024	0.027	0.015 (19)
390	0.031	0.028	

*All published values are at 25°C.

values at the intermediate wavelengths, 337 and 351 nm, were approximately half those previously reported at these wavelengths (337 nm [19], 351 nm [13]). The reasons for the differences are unknown, but they may be partly due to uncertainties in the percentage of OH radical reacting with BA.

REFERENCES

1. Hatchard, C. G. and C. A. Parker (1956) A new sensitive chemical actinometer: II. Potassium ferrioxalate as a standard chemical actinometer. *Proc. R. Soc.* **235A**, 518–536.
2. Zepp, R. G., M. M. Gumz, W. L. Miller and H. Gao (1998) Photoreaction of valerophenone in aqueous solution. *J. Phys. Chem.* **102**, 5716–5723.
3. Dulin, D. and T. Mill (1982) Development and evaluation of sunlight actinometers. *Environ. Sci. Technol.* **16**, 815–820.
4. Meyerstein, D. and A. Treinin (1961) Absorption spectra of NO$_3^-$ in solution. *Trans. Faraday Soc.* **57**, 2104–2112.
5. Maria, H. J., J. R. McDonald and S. P. Mcglynn (1973) Electronic absorption spectrum of nitrate ion and boron trihalides. *J. Am. Chem. Soc.* **95**, 1050–1056.
6. McConnell, H. (1952) Effects of polar solvents on the absorption frequency of n → π electronic transitions. *J. Chem. Phys.* **20**, 700–704.
7. McEwen, K. L. (1961) Electronic structures and spectra of some nitrogen-oxygen compounds. *J. Chem. Phys.* **34**, 547–555.
8. Rotlevi, E. and A. Treinin (1965) The 300-mμ band of NO$_3^-$. *J. Phys. Chem.* **69**, 2645–2648.
9. Shuali, U., M. Ottolenghi, J. Rabani and Z. Yelin (1969) On the photochemistry of aqueous nitrate solutions excited in the 195-nm band. *J. Phys. Chem.* **73**, 3445–3451.
10. Daniels, M., R. V. Meyers and E. V. Belardo (1968) Photochemistry of the aqueous nitrate system. I. Excitation in the 300-mμ band. *J. Phys. Chem.* **72**, 389–398.
11. Zafiriou, O. C. and M. B. True (1979) Nitrate photolysis in seawater by sunlight. *Mar. Chem.* **8**, 33–42.
12. Zepp, R. G., J. Hoigné and H. Bader (1987) Nitrate-induced photooxidation of trace organic chemicals in water. *Environ. Sci. Technol.* **21**, 443–450.
13. Zellner, R., M. Exner and H. Herrmann (1990) Absolute OH quantum yields in the laser photolysis of nitrate, nitrite and dissolved H$_2$O$_2$ at 308 and 351 nm in the temperature range 278–353 K. *J. Atmos. Chem.* **10**, 411–425.
14. Warneck, P. and C. Wurzinger (1988) Product quantum yields for the 305-nm photodecomposition of NO$_3^-$ in aqueous solution. *J. Phys. Chem.* **92**, 6278–6283.
15. Mark, G., H. G. Korth, H. P. Schuchmann and C. von Sonntag (1996) The photochemistry of aqueous nitrate ion revisited. *J. Photochem. Photobiol.* **101**, 89–103.
16. Brekken, J. F. and P. L. Brezonik (1997) Indirect photolysis of acetochlor: rate constant of a nitrate mediated hydroxyl radical reaction. *Chemosphere* **35**, 2699–2704.
17. Strickler, S. J. and M. Kasha (1963) Solvent effects on the electronic absorption spectrum of nitrite ion. *J. Am. Chem. Soc.* **85**, 2899–2901.
18. Treinin, A. and E. Hayon (1970) Absorption spectra and reaction kinetics of NO$_2$, N$_2$O$_3$, and N$_2$O$_4$ in aqueous solution. *J. Am. Chem. Soc.* **92**, 5821–5828.
19. Zafiriou, O. C. and R. Bonneau (1987) Wavelength-dependent quantum yield of OH radical formation from photolysis of nitrite ion in water. *Photochem. Photobiol.* **45**, 723–727.
20. Bates, H. G. C. and N. Uri (1953) Oxidation of aromatic compounds in aqueous solution by free radicals produced by photo-excited electron transfer in iron complexes. *J. Am. Chem. Soc.* **75**, 2754–2759.
21. Armstrong, W. A. and D. W. Grant (1958) A highly sensitive chemical dosimeter for ionizing radiation. *Nature* **162**, 747.
22. Armstrong, W. A., B. A. Black and D. W. Grant (1960) The radiolysis of aqueous calcium benzoate and benzoic acid solutions. *J. Phys. Chem.* **64**, 1415–1419.
23. Matthews, R. W. and D. F. Sangster (1965) Measurement by benzoate radiolytic decarboxylation of relative rate constants for hydroxyl radical reactions. *J. Phys. Chem.* **69**, 1938–1946.
24. Loeff, I. and A. J. Swallow (1964) On the radiation chemistry of concentrated aqueous solutions of sodium benzoate. *J. Phys. Chem.* **68**, 2470–2475.
25. Klein, G. W., K. Bhatia, V. Madhavan and R. H. Schuler (1975) Reaction of ·OH with benzoic acid. Isomer distribution in the radical intermediates. *J. Phys. Chem.* **79**, 1767–1774.
26. Oturan, M. A. and J. Pinson (1995) Hydroxylation by electrochemically generated OH radicals. Mono- and polyhydroxylation of benzoic acid: products and isomers' distribution. *J. Phys. Chem.* **99**, 13948–13954.
27. Zhou, X. and K. Mopper (1990) Determination of photochemically produced hydroxyl radicals in seawater and freshwater. *Mar. Chem.* **30**, 71–88.
28. Kuhn, H. J., S. E. Braslavsky and R. Schmidt (1989) Chemical actinometry. *Pure Appl. Chem.* **61**, 187–210.
29. Barker, G. C., P. Fowles and B. Stringer (1970) Pulse radiolytic induced transient electrical conductance in liquid solutions. Part 2. Radiolysis of aqueous solutions of NO$_3^-$, NO$_2^-$, and Fe(CN)$_3^{3-}$. *Trans. Faraday Soc.* **66**, 1509–1519.
30. Gaffney, J. S., N. A. Marley and M. M. Cunningham (1992) Measurement of the absorption constants for nitrate in water between 270 and 335 nm. *Environ. Sci. Technol.* **26**, 207–209.
31. Zuo, Y. and Y. Deng (1998) The near UV absorption constants for nitrite ion in aqueous solution. *Chemosphere* **36**, 181–188.
32. Grasshoff, K., M. Ehrhardt and K. Kremling (1983) *Methods of Seawater Analysis,* pp. 139–142. Verlag Chemie, Weinheim.
33. Buxton, G. V., C. L. Greenstock, W. P. Helman and A. B. Ross (1988) Critical review of rate constants for reactions of hydrated electrons, hydrogen atoms, and hydroxyl radicals in aqueous solutions. *J. Phys. Chem. Ref. Data* **17**, 513–887.
34. Farhataziz and A. B. Ross (1977) Selected specific rates of reactions of transients from water in aqueous solution III. *Natl. Std. Ref. Data Sys.,* pp. 1–113.
35. Strickler, S. J. and M. Kasha (1964) *Molecular Orbitals in Chemistry, Physics and Biology.* Academic Press, New York.
36. Mopper, K. and X. Zhou (1990) Hydroxyl radical photoproduction in the sea and its potential impact on marine processes. *Science* **250**, 661–664.
37. Vaughan, P. P. and N. V. Blough (1998) Photochemical formation of hydroxyl radical by constituents of natural waters. *Environ. Sci. Technol.* **32**, 2947–2953.